INTERNATIONAL JOURNAL FOR NUMERICAL AND ANALYTICAL METHODS IN GEOMECHANICS
Int. J. Numer. Anal. Meth. Geomech. 2012; **36**:236–248
Published online 11 March 2011 in Wiley Online Library (wileyonlinelibrary.com). DOI: 10.1002/nag.1021

Factor of safety in a partially saturated slope inferred from hydro-mechanical continuum modeling

Ronaldo I. Borja[1,*,†], Joshua A. White[2], Xiaoyu Liu[1] and Wei Wu[3]

[1]*Department of Civil and Environmental Engineering, Stanford University, Stanford, CA 94305, U.S.A.*
[2]*Computational Geosciences Group, Lawrence Livermore National Laboratory, Livermore, CA 94551, U.S.A.*
[3]*Institut für Geotechnik, Universität für Bodenkultur, Feistmantelstrasse 4, 1180 Vienna, Austria*

SUMMARY

Rainfall weakens an earth slope and triggers mass movement. Relevant triggering mechanisms are complex and include reduction of capillary pressure due to increased saturation and frictional drag on the sediment induced by fluid flow. Physics-based continuum models utilizing modern computational tools are useful for understanding the mechanisms of deformation in partially saturated slopes; however, they do not provide a scalar indicator called 'factor of safety' that measures the potential of a given slope for mass movement. In the present work, we employ sequential calculations consisting of a physics-based finite element model that couples solid deformation with fluid flow to quantify the stress and deformation fields in a steep hillside slope subjected to rainfall infiltration. This is followed by a limit-equilibrium calculation based on the method of slices that evaluates the desired factor of safety. The field condition investigated is similar to the steep experimental catchment CB1 near Coos Bay, Oregon, which failed as a large debris flow from heavy rainfall.

Received 1 July 2010; Revised 14 October 2010; Accepted 23 December 2010

KEY WORDS: partially saturated soil; hydromechanical model; slope stability

1. INTRODUCTION

Landslides induced by heavy rainfall cause widespread damage and occasional loss of life. Relevant triggering mechanisms are complex and include reduction of capillary pressure, surface and subsurface fluid flow, irregular topography, and local drainage boundary conditions [1, 2]. Very recently, a three-dimensional physics-based continuum model has been proposed that captures the coupled solid deformation–fluid flow processes in variably saturated slopes [3, 4]. The model is based on a mixed finite element formulation relating the solid displacement and pore pressure degrees of freedom, and realistically quantifies stresses and pore pressures responsible for triggering slope failure. However, continuum modeling cannot calculate a scalar indicator called 'factor of safety' that is used universally as a measure of proximity of slope conditions to failure. On the other hand, limit-equilibrium solutions, such as those utilizing the method of slices, do calculate a factor of safety but cannot accommodate the complex three-dimensional hillslope processes.

This paper describes a methodology for coupling physics-based continuum modeling with limit-equilibrium calculations for a steep hillside slope subjected to rainfall infiltration. The continuum model solves the partial differential equations governing the hydro-mechanical processes in a

*Correspondence to: Ronaldo I. Borja, Department of Civil and Environmental Engineering, Stanford University, Stanford, CA 94305, U.S.A.
†E-mail: borja@stanford.edu

partially saturated porous medium, as well as accommodates relevant constitutive properties including the impact of increased saturation on the mechanical properties of the porous material. The stress and pore pressure fields generated by the continuum model are interfaced with a limit-equilibrium solution based on the method of slices to calculate the desired factor of safety. The case study analyzed has a peculiar topography that challenges the accuracy and sensitivity of the sequential calculations to small perturbations in the problem geometry. Remarkably, the critical yield zone predicted by the continuum model agrees well with the critical slip surface identified by the limit-equilibrium solution, suggesting that interfacing the two solutions is a meaningful approach for studying the deformation and stability properties of the slope.

The specific case study considered in this paper is similar to the highly instrumented Coos Bay experimental catchment CB1, which was chosen as a hillslope-scale 'laboratory' for conducting hydrologic sprinkling experiments [5, 6]. The CB1 slope failed as a large debris flow due to heavy rain in November 1996, raising some scientific questions related to the geotechnical aspects of the site. The slope at CB1 is steep, on the order of 43°. The sediment is colluvium, a surficial soil derived from the weathering of fresh bedrock located only 1.5–2 m deep below the slope face. We could have modeled the slope as a one-dimensional sliding layer on a steep incline; however, the large debris flow that occurred in 1996 was far from being one-dimensional. This raises important questions regarding possible effects of local surface topography, saturation, fluid flow, and three-dimensional geometry on the mechanism of slope failure at CB1.

Despite much effort to constrain the topography, hydrologic aspects, and boundary conditions at the CB1 site, much uncertainty remains about this experimental catchment. Sources of uncertainty include the highly fractured bedrock that could have served as a source or sink for fluids, and the unknown variability of the sediment properties at the site. Because of these uncertainties, it would be more prudent to associate the results of this analysis to a slope with similar configuration and scale to CB1, but not to the slope at CB1 itself. The scope of this paper is limited to understanding the timing, location, and relevant triggering mechanism of slope failure for a given rainfall intensity. Aspects related to post-failure condition, such as distance traveled by the landslide and its final depositional configuration, are not covered in this paper.

2. PROBLEM DEFINITION AND METHODS OF ANALYSIS

The CB1 experimental catchment is located along Mettman Ridge approximately 15 km north of Coos Bay in the Oregon Coast Range. CB1 is a 51-m long (860 m^2) unchanneled valley, with a north-facing aspect and an average slope of 43° (see Figure 1). Three sprinkling experiments were conducted at CB1: in May 1990 at 1.5 mm/h for 6 days; in May 1990 at 3.0 mm/h for 4 days; and in May 1992 at 1.7 mm/h for 7 days. The instrumentation at CB1 included an exhaustive grid of rain gauges, piezometers, tensiometers, TDR wave guide pairs (for estimating soil–water content), lysimeters, meteorological sensors (on a tower), atmometers, and weirs. In November 1996, the CB1 slope failed as a large debris flow after an intense natural rainfall. Figure 2 shows the hyetograph at CB1 and at nearby North Bend, Oregon airport during the week of intense rainfall. The instrumentation at CB1 provides one of the most comprehensive hydrologic response data sets in existence for a steep, deforested catchment that failed by debris flow.

The continuum model utilized to analyze the slope satisfies balance of mass and balance of linear momentum for solid, water, and air [4, 7]. For the unsaturated zone, we calculate the effective stress from the Bishop stress [8] but with the Bishop parameter replaced by the degree of saturation. The first law of thermodynamics justifies this definition of effective stress for constitutive modeling of unsaturated porous material response [9, 10]. The bedrock layer at CB1 is very shallow, on the order of 1–2 m below the colluvium; hence, we simply assume a passive pore air pressure condition in the sediment, i.e. the pore air pressure is equal to the atmospheric pressure throughout the simulation. However, the colluvium was initially unsaturated and subjected to a propagating wetting front. We assume flow in the saturated and unsaturated regions to be governed by Darcy's law and use the wetting curve of the Van Genuchten [11] relation to define the evolution of

DOI: 10.1002/nag

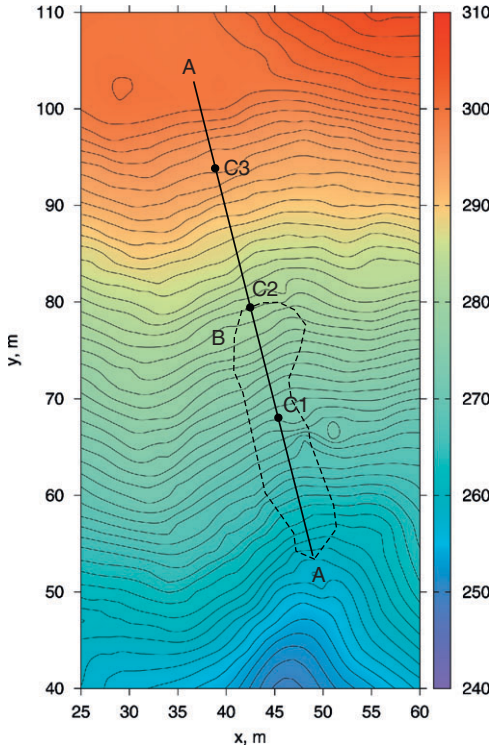

Figure 1. Topographic map for CB1 experimental catchment. Two-dimensional plane strain condition is assumed along section A-A for the physics-based and limit-equilibrium simulations. Dashed curve B delineates the extent of debris flow zone from the event of November 1996. C1, C2, and C3 are inflection points discussed in the simulations. Color bar is elevation in meters.

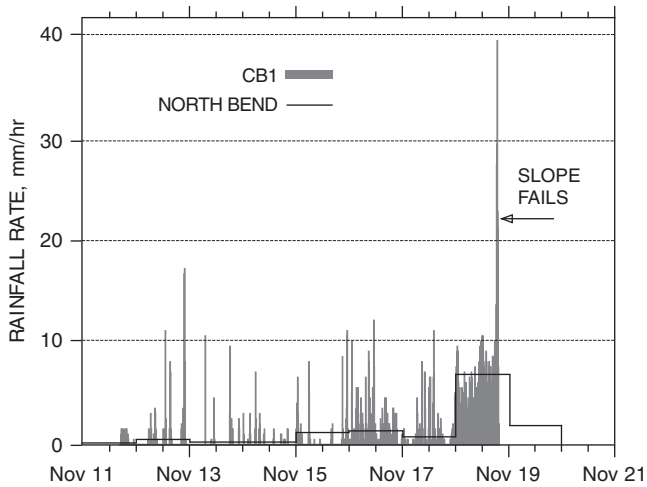

Figure 2. Hyetograph in 1996 at CB1 and daily rainfall averages from nearby North Bend, Oregon airport.

hydraulic conductivity in the unsaturated zone. This assumption is justified by a recent article [12] suggesting that the wetting soil–water retention curve is appropriate for the present study.

Owing to the uncertainties in the boundary conditions and problem geometry of the test problem, we resort to plane strain finite element modeling on section A-A of the slope that cuts through the middle of the debris flow zone B shown in Figure 1. Figures 3 and 4 show the finite element mesh for this section. We use stabilized four-node quadrilateral mixed finite elements for displacement and pore pressure interpolations [13] to fully couple fluid flow with solid deformation in the

DOI: 10.1002/nag

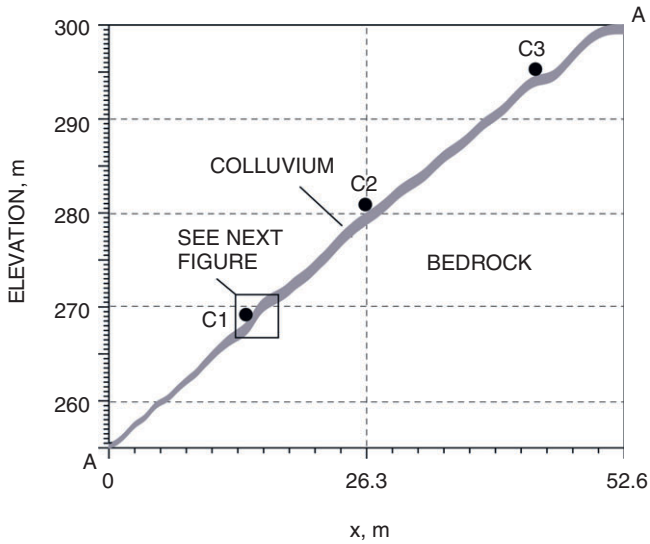

Figure 3. Slope elevation through Section A-A (see Figure 1). Shaded region is colluvium underlain by fractured bedrock. C1, C2, and C3 are inflection points discussed in the simulations.

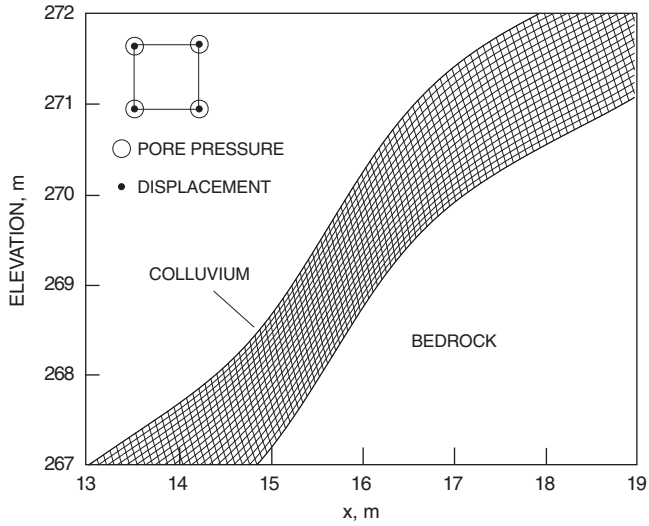

Figure 4. Finite element discretization in the neighborhood of inflection point C1. Each node on a stabilized mixed element has three degrees of freedom: two displacement components and one pore water pressure.

colluvium. We assume the underlying bedrock to be rigid. We consider simplified rainfall and fluid flow scenarios that closely match the hyetograph for CB1, as well as investigate various possible fluid flow boundary conditions, including prescribing a fluid flux over a segment of the fractured bedrock underneath the colluvium to investigate its effect on slope stability. We prescribe rainfall as a boundary condition on the slope surface in the form of a normal flux into the slope face.

For each stress configuration, we run limit-equilibrium analyses based on the method of slices to determine the factor of safety against slope failure as well as compare the failure zones generated by the continuum and limit-equilibrium solutions. We employ two methods of slope stability analysis: Spencer's [14] method and the modified Bishop [15] method. Spencer's method assumes parallel inter-slice resultant forces, and results in a system of linear equations that is statically determinate. The modified Bishop method assumes that the vertical components of inter-slice forces are zero, and results in a system of linear equations that is over-constrained to the first degree (i.e. there is

DOI: 10.1002/nag

one unsatisfied equation of equilibrium). In general, Spencer's method gives slightly higher factor of safety than the modified Bishop method for a given slope.

We use a commercial slope stability analysis code SLOPE/W to search for the most critical failure surface and calculate the corresponding factor of safety. This code calculates the shear strength on the failure surface from the equation [16]

$$\tau_{\max} = c' + (\sigma - u_a)\tan\phi' + (u_a - u_w)\tan\phi^b, \tag{1}$$

where c' and ϕ' are the effective cohesion and angle of internal friction, respectively, σ is the normal stress on the failure surface, u_a and u_b are the pore air and pore water pressures, respectively, and ϕ^b is an angle defining the increase in shear strength for an increase in matrix suction $s = u_a - u_w$. The code also assumes the passive air condition, $u_a = 0$, and thus the above equation reduces to

$$\tau_{\max} = c' + \sigma' \tan\phi', \tag{2}$$

where σ' is an effective normal stress that has the form

$$\sigma' = \sigma - u_w \frac{\tan\phi^b}{\tan\phi'}. \tag{3}$$

This expression can be reconciled with Bishop's definition of effective normal stress [8], with Bishop's parameter replaced by the degree of saturation S_r, if one takes $\tan\phi^b / \tan\phi' = S_r$, or

$$\phi^b = \tan^{-1}(S_r \tan\phi'). \tag{4}$$

Bishop's effective stress, with the Bishop parameter replaced by the degree of saturation S_r, is consistent with the first law of thermodynamics [7, 9, 17].

SLOPE/W accommodates difficult and unusual problem geometry such as those encountered in CB1. Since the colluvium–bedrock interface at CB1 is relatively straight and the colluvium layer is very thin, the code assumes that the critical failure surface passes through a segment of the sediment–bedrock interface (i.e. it does not carve into the bedrock) and emerges at two points on the slope surface. In the following discussions we shall call the upslope intersection of the failure surface with the slope face as the entry point, and the downslope intersection as the exit point. Prediction of the location of the entry point is critical in the assessment of the accuracy of the model inasmuch as a vertical scarp would be expected to form naturally at this point, thereby allowing a comparison of the calculated mechanism of deformation with the location of the scarp zone that was formed from the actual failed slope at CB1.

SLOPE/W does not accept point-wise values of pore pressures on the failure surface but instead calculates them based on the vertical distance to a prescribed phreatic surface, without accounting for the head loss that results from a non-horizontal phreatic surface. This procedure could grossly overestimate the pore water pressure on the failure surface particularly for steep slopes. To correct this error, we prescribe a reduced height of the phreatic surface (relative to what was calculated by the hydro-mechanical continuum simulation) by a factor of $\cos^2\alpha$, where α is the slope angle. Thus, if the continuum model calculates a vertical distance h_p of the phreatic surface from a point on the failure surface, then we input a reduced height of $h_p \cos^2\alpha$ into the limit-equilibrium model. In the examples that follow, we report pore pressure values determined by the continuum model and used as input by the limit-equilibrium solution to calculate the factor of safety.

3. MODEL PARAMETERS AND NUMERICAL PROCEDURES

For the continuum simulation, we model the sediment in the slope as a non-associative elasto-plastic Mohr–Coulomb material. Using a critical state constitutive formulation [18, 19] may not improve the modeling much since the slope is steep and all the stress points lie on the dilative side of the yield surface. The relevant material parameters are friction angle $\phi' = 40^\circ$, dilatancy angle $\psi = 25^\circ$, cohesion $c' = 4.0\,\text{kPa}$, elastic bulk modulus $K = 50\,\text{MPa}$, Poisson's ratio $\nu = 0.25$, porosity

DOI: 10.1002/nag

$n = 0.50$, and intrinsic solid density $\rho_s = 2.2\,\mathrm{Mg/m^3}$. While the colluvium in CB1 likely exhibited a complicated hardening and/or softening behavior, we do not have sufficient experimental data to calibrate this feature of the mechanical response, and therefore we assume that the material parameters remain constant with plastic deformation (perfect plasticity). For the suction/saturation model, we consider a non-hysteretic van Genuchten model defining the wetting part of the hydrologic response. The relevant parameters are intrinsic permeability $k = 3.5 \times 10^{-11}\,\mathrm{m^2}$, dynamic viscosity $\eta = 1.0 \times 10^{-6}\,\mathrm{kPa\text{-}s}$, fluid density $\rho_w = 1.0\,\mathrm{Mg/m^3}$, residual saturation $\psi_0 = 0.32$, maximum saturation $\psi_1 = 1.0$, scaling pressure $s_a = 0.4\,\mathrm{kPa}$, and shape constant $n = 3.0$. See [3] for an elaboration of these model parameters and how their values were determined for the CB1 site.

We fix the displacements at the bottom bedrock boundary and accommodate all inelastic deformation as bulk plastic deformation within the colluvium. Alternatively, a frictional boundary condition could have been considered to represent the contact kinematics on the colluvium/bedrock interface, but this was not pursued in this study. At the beginning of the simulations, we prescribe a uniform initial pressure of $-1.5\,\mathrm{kPa}$ within the colluvium representing an approximate initial saturation condition in the slope prior to the major rainfall event. While this may be considered as a gross simplification, previous studies [12] suggest that the ultimate failure is relatively insensitive to the rainfall history prior to the main rainfall event.

We use a gravity loading phase to calibrate the initial *in situ* stress conditions within the slope. Once these initial stresses are computed, we reset the displacements to zero and begin the coupled phase of the simulation. To simulate a rainfall event, we prescribe a fluid flux q at the ground surface (natural boundary condition) and apply this flux continually unless a seepage face condition is detected—i.e. fluid exfiltrates from the bottom of the slope—at which point we switch the boundary at these points to a fixed pressure $p = 0$ (essential boundary condition). Switching the boundary conditions on the slope face from a Neumann-type (natural) to a Dirichlet-type (essential) ensures that the proper flow physics is maintained at the infiltration/exfiltration boundary throughout the simulations.

The hyetograph shown in Figure 2 indicates a peak rainfall rate of nearly 40 mm/h, which is about an order of magnitude higher than typical peak rainfall rates at CB1 during 7 years of observation [12]. Prior to this peak period, rainfall persisted at an average rate of 6 mm/h over a 24-h period, which could have contributed to conditioning the soil saturation to subsequent failure. However, we see that the peak rainfall was so intense that it clearly was the main trigger to slope failure. Note that the hyetograph shown in Figure 2 has a highly erratic variation. Considering that we ignored the effects of three-dimensional geometry in the simulations, it is doubtful that much can be gained by capturing the actual erratic time history of the rainfall, and hence we simply consider a rainfall sequence consisting of a uniform 'spin-up' rainfall of 6 mm/h for 24 h, followed by a uniform rainfall of 40 mm/h up until failure.

4. RESULTS FOR SIMPLIFIED CB1 RAINFALL

At a prescribed rainfall of 6 mm/h for 24 h, the continuum simulations did not detect any failure in the slope. However, at a prescribed flux of 40 mm/h following the spin-up rainfall, the slope 'failed' after 1.7 h of exposure to this intense rain. 'Failure' in the continuum sense is defined by a localized extensional shear zone fully propagating from the colluvium–bedrock interface all the way up to the slope face. At this point, the Newton iterations stopped converging. While the lack of convergence in Newton iterations does not necessarily imply onset of instability, the fact that the yield zone has fully propagated to the slope face at the moment when the Newton iterations stopped converging suggests that a failure mechanism indeed has formed, thereby inhibiting the continuum solution from finding an equilibrium configuration for the current loading condition.

Figures 5 and 6 show two extensional shear zones forming nearly simultaneously at the moment of 'failure,' the first at point C1 with coordinate $x = 17\,\mathrm{m}$ on plane A-A, and the second at point C2 with coordinate $x = 27\,\mathrm{m}$. Both locations are inflection points on the slope surface. For reference, the figure also shows a third inflection point C3 located much farther upslope, at $x = 44\,\mathrm{m}$, that was

DOI: 10.1002/nag

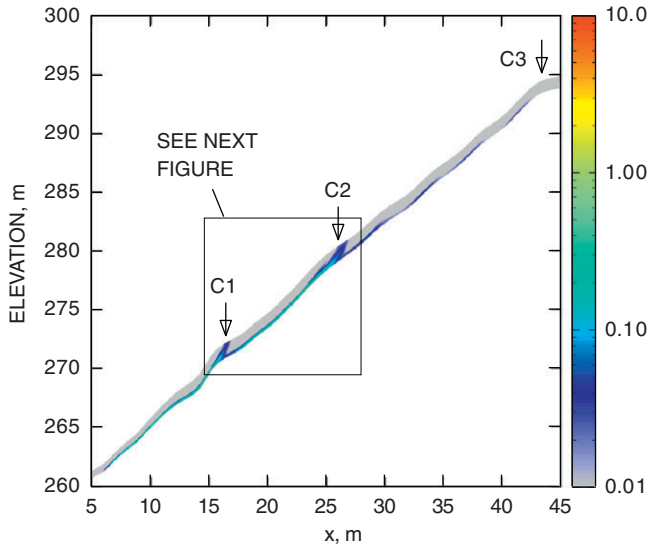

Figure 5. Extensional shear zones predicted by the hydro-mechanical continuum model for rainfall rates of 6 mm/h for 24 h followed by 40 mm/h for 1.7 h. Inflection point C2 is the upslope scarp location at CB1. Color bar is plastic strain in percent.

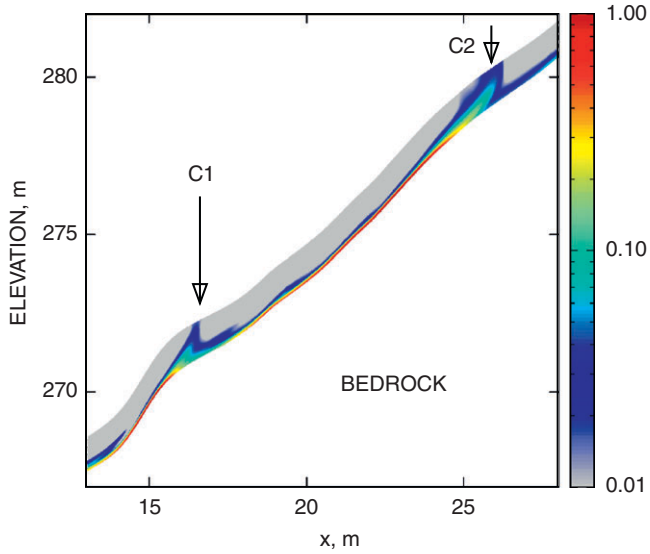

Figure 6. Magnified view of extensional shear zones predicted by the hydro-mechanical continuum model for rainfall rates of 6 mm/h for 24 h followed by 40 mm/h for 1.7 h. Localized plastic zone defines a multiple block failure mechanism. Color bar is plastic strain in percent.

not triggered by this rainfall but would prove more critical for a different rainfall scenario discussed later. It is worthy of note that point C2 coincides with the scarp zone that developed in CB1 from the rainfall of 1996, see Figure 1. The fact that a scarp zone developed in the neighborhood of an inflection point suggests that bedrock topography does have a strong influence on the kinematics of slope failure. The failure mechanism shown in Figures 5 and 6 is similar to multiple block failure described by Varnes [20], in contrast to the classic spoon-shape failure mechanism considered by the limit-equilibrium solution.

Figure 7 shows the calculated pore water pressures on the colluvium–bedrock interface. The values of the pore water pressures were all positive, implying a fully saturated condition. Higher pore water pressures were calculated on the lower portion of the slope after time $t = 24$ h as the

DOI: 10.1002/nag

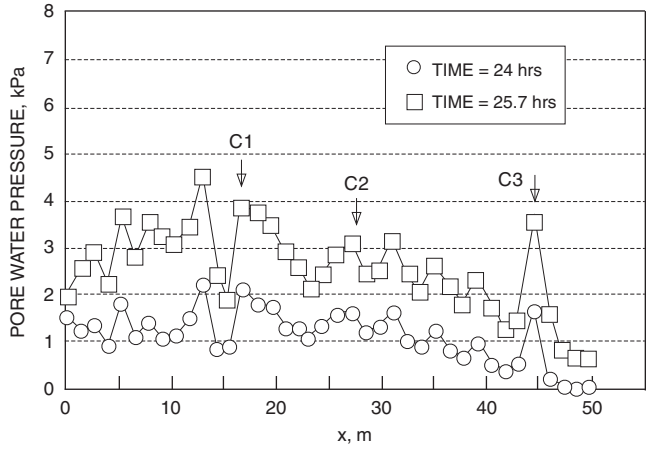

Figure 7. Pore water pressure on colluvium–bedrock interface after subjecting the slope to 6 mm/h rain for 24 h (open circle) followed by 40 mm/h rain for 1.7 h (open square) representing the simplified CB1 rain leading to the 1996 slope failure. Numerical simulations predicted a scarp zone at C2, agreeing with the scarp zone in CB1.

groundwater was given sufficient time to flow downhill. However, the more intense rain caused the pore water pressures at time $t = 25.7$ h to increase almost uniformly everywhere except near the bottom of the slope where the surface topography was flatter, and therefore the pore water pressures were constrained by the hydrostatic values. The erratic variation of the pore water pressure was due to the irregular surface topography, as evidenced by the peaks and valleys of the pore pressures being sharpest near the inflection points C1, C2, and C3.

Limit-equilibrium solution searches for the critical failure surface that gives the minimum factor of safety. By definition, there is only one critical failure surface in a limit-equilibrium solution; however, the continuum solution repeatedly identified inflection points C1, C2, and C3 as potential zones of failure initiation, and hence we investigate the presence of 'local minima' on the factor of safety in the neighborhood of these inflection points. The algorithm used to search for a local minimum in the neighborhood of an inflection point is based on the entry/exit windows search option of SLOPE/W. Here, we prescribe sufficiently long windows or spans on the slope face through which the failure surfaces could possibly pass. We then investigate if a local minimum on the factor of safety would occur inside each of these windows.

Results of the limit-equilibrium search are summarized in Figure 8. After 24 h of rain at 6 mm/h, the critical failure surface was detected to pass through inflection point C2. The calculated factors of safety are 1.260 with Spencer's method and 1.259 with the modified Bishop method. After 1.7 h of additional rain at 40 mm/h, the calculated factors of safety decreased to 1.122 with Spencer's method and 1.121 with the modified Bishop method. The predicted scarp zone remained in the neighborhood of inflection point C2, in agreement with the continuum solution and the actual position of the scarp zone observed for CB1. The simulations did not detect any local minimum on the factor of safety in the neighborhood of inflection points C1 or C3—when restricted to pass through the windows containing these inflection points, the search algorithm simply converged to the edge of each window closest to inflection point C2.

A rough check on the factor of safety may be inferred from a simplified one-dimensional representation of the slope. With the bedrock located at a vertical distance of H from the slope face, the factor of safety is given by

$$\mathrm{FS} = \frac{\tan\phi'}{\tan\beta} + \frac{c'}{\gamma H \sin\beta\cos\beta} - \frac{u\tan\phi'}{\gamma H \cos\beta\sin\beta}, \tag{5}$$

where c' and ϕ' are, respectively, the effective cohesion and friction angle on the sediment–bedrock interface, γ is the total unit weight of the sliding sediment, u is the average pore water pressure

DOI: 10.1002/nag

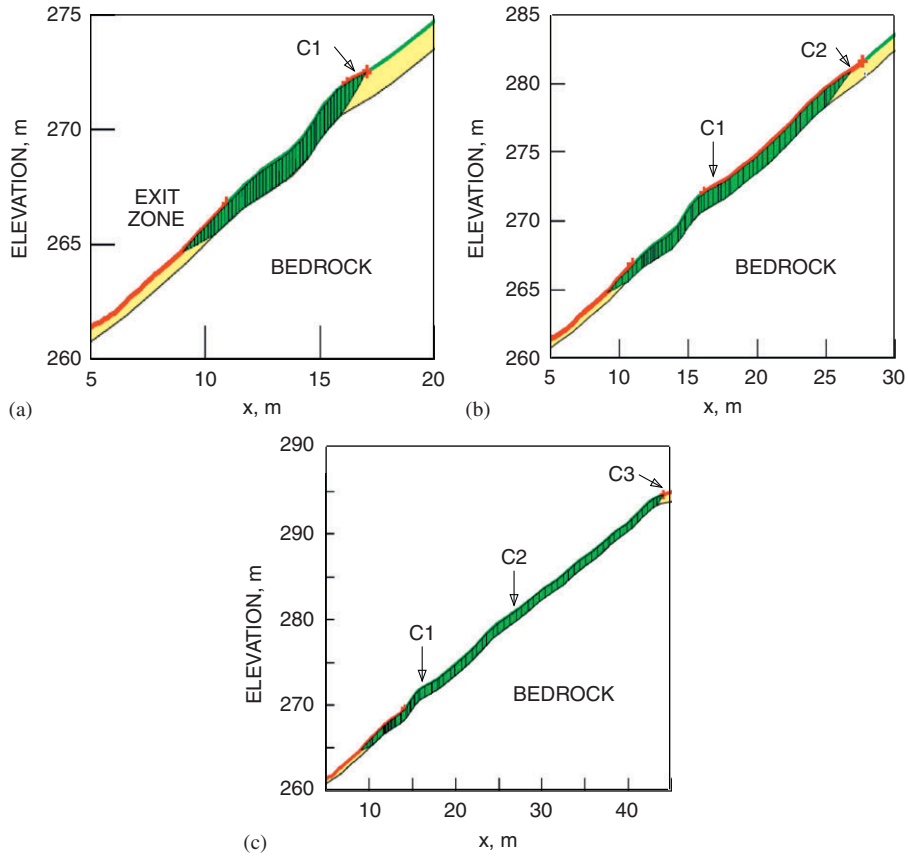

Figure 8. Search for local minima on the factor of safety in the neighborhood of (a) inflection point C1; (b) inflection point C2; and (c) inflection point C3. No local minimum is found in the neighborhood of inflection points C1 and C3 for the simplified CB1 rainfall simulation.

on the failure surface, and β is the slope angle. In the above equation, the failure surface is assumed to coincide with the sediment–bedrock interface. Between inflection points C1 and C3, the average slope angle is $\beta = 39.4^\circ$, the average unit weight of the sediment is $\gamma = 15.7\,\text{kN/m}^3$, and the average height of the slope is $H = 0.95\,\text{m}$. For an effective cohesion $c' = 4\,\text{kPa}$ and an effective friction angle $\phi' = 40^\circ$ on the sediment–bedrock interface, the factor of safety is given by the equation $\text{FS} = 1.594 - 0.1148u$ (u in kPa). From Figure 7, the average pore water pressures between C1 and C3 are 1.2 kPa after 24 h, and 3 kPa after 25.7 h. The corresponding factors of safety are 1.45 and 1.25, respectively. These numbers underestimate the failure potential of the slope. In fact, even if we take the maximum pore water pressures of 2 kPa after 24 h, and 4 kPa after 25.7 h (see Figure 7), the calculated factor of safety would still be 1.364 and 1.135, respectively. Clearly, the one-dimensional model neither can account for the local dips and bumps in the surface topography, nor can it predict the location of the scarp zone, and therefore is inadequate for the present problem.

5. RESULTS FOR HYPOTHETICAL RAINFALL SIMULATIONS

In the previous section, we captured the slope failure mechanism at CB1 using a simplified rainfall for this experimental catchment. In this section, we show that different rainfall histories do produce different failure mechanisms. To this end, we subject the same slope to two hypothetical rainfall histories: rainfall A at 14 mm/h for 13.6 h, and rainfall B at 50 mm/h for 2.5 h. In both cases, the

DOI: 10.1002/nag

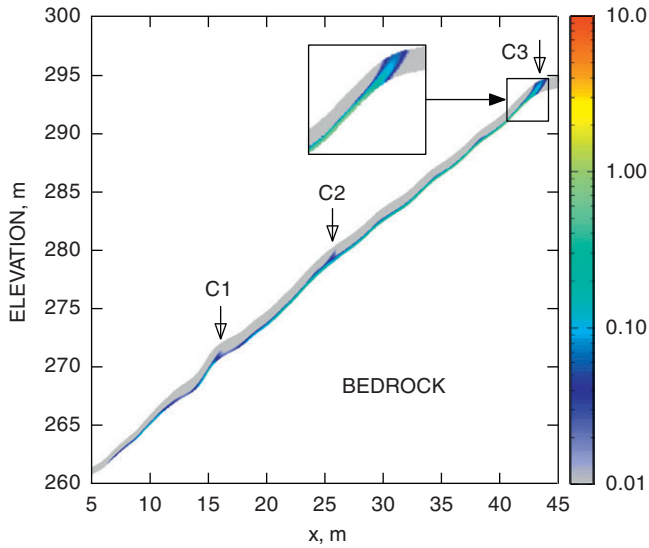

Figure 9. Extensional shear zones predicted by the hydro-mechanical model for a rainfall rate of 50 mm/h for 2.5 h. A primary scarp zone is developed at inflection point C3. Color bar is plastic strain in percent.

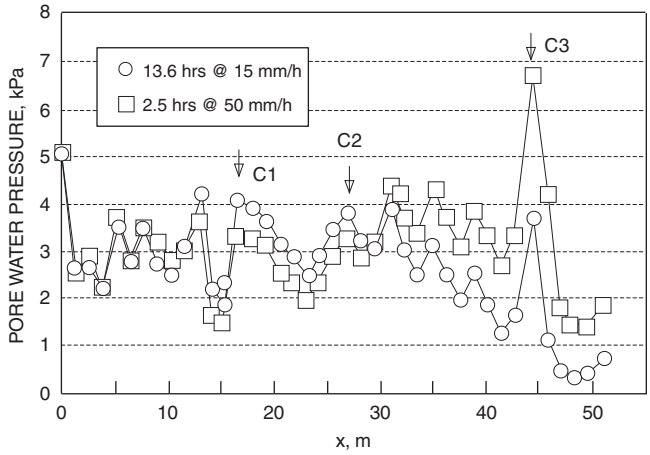

Figure 10. Pore water pressures on colluvium–bedrock interface after subjecting the slope to 13.6 h of rain at 15 mm/h (open circle) and 50 mm/h of rain for 2.5 h (open square). Numerical simulations predicted a scarp zone at C2 for the former and at C3 for the latter.

sediment had an initial pore water pressure of −1.5 kPa, and no previous rain was applied. The two rainfall loadings caused the slope to fail in two different ways.

Rainfall A induces a primary scarp zone at inflection point C2 similar to that shown in Figures 5 and 6. In contrast, rainfall B generates a primary scarp zone much farther upslope, near inflection point C3, as shown in Figure 9. Figure 10 reveals the reason behind the two distinct failure mechanisms: For rainfall B the wetting front could not propagate quickly enough into the lower portion of the slope, causing the pore water pressures to build up in the vicinity of C3 and causing the slope to fail there. Note that point C3 is inconsistent with the observed scarp zone for CB1. We thus see that the initial pre-wetting rainfall plays a crucial role in defining the debris flow zone. For CB1 the initial pre-wetting was responsible for saturating the lower portion of the slope prior to the 40 mm/h pulse, and without it the slope could have developed a scarp zone at C3.

DOI: 10.1002/nag

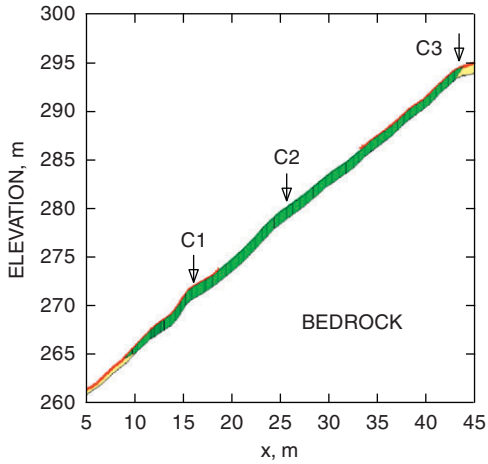

Figure 11. Critical failure surface using the entry–exit option of SLOPE/W for a hypothetical rainfall rate of 50 mm/h for 2.5 h without previous rainfall. The search predicted a scarp zone at inflection point C3.

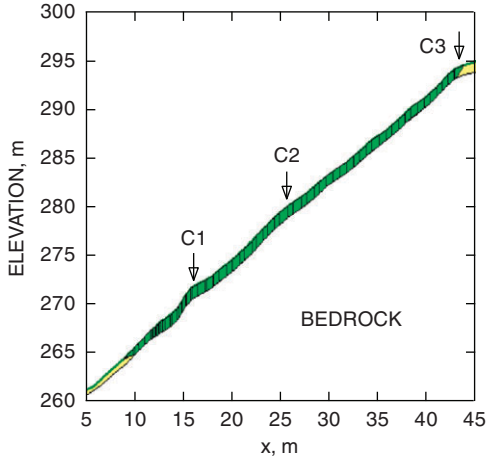

Figure 12. Critical failure surface using the grid-radius option of SLOPE/W for a hypothetical rainfall rate of 50 mm/h for 2.5 h without previous rainfall. The search predicted a scarp zone at inflection point C3.

For rainfall A, the limit-equilibrium solution predicted a scarp zone at C2, in agreement with the continuum solution. For rainfall B, the limit-equilibrium solution predicted a scarp zone at C3, also in agreement with the continuum solution. In running the limit-equilibrium simulations, we used the entry/exit and grid/radius algorithms of SLOPE/W, and for rainfall B the results are shown in Figures 11 and 12. Both search algorithms identified the same scarp zone, i.e. at C3. The calculated factors of safety are 1.031 (Spencer) and 1.029 (modified Bishop) under rainfall A, and 1.146 (Spencer and modified Bishop) under rainfall B.

Finally, we investigate the effect on slope stability of an upward seepage emanating from the fractured bedrock. As mentioned in the Introduction, this is a source of uncertainty at CB1, inasmuch as the bedrock could have served as a source or sink for fluids due to the high fracture density. To this end, we prescribe a normal fluid flux over a segment of the bedrock as shown in Figures 13 and 14. Acting alone, the upward flux has to reach a magnitude as high as 100 mm/h for 2.5 h to generate a scarp zone through inflection point C1. Clearly, this is an unreasonably high number. Therefore, we conclude that an upward seepage needs to act in combination with some rainfall loading on the slope surface in order to have an impact on the triggering of failure on a slope similar to CB1.

DOI: 10.1002/nag

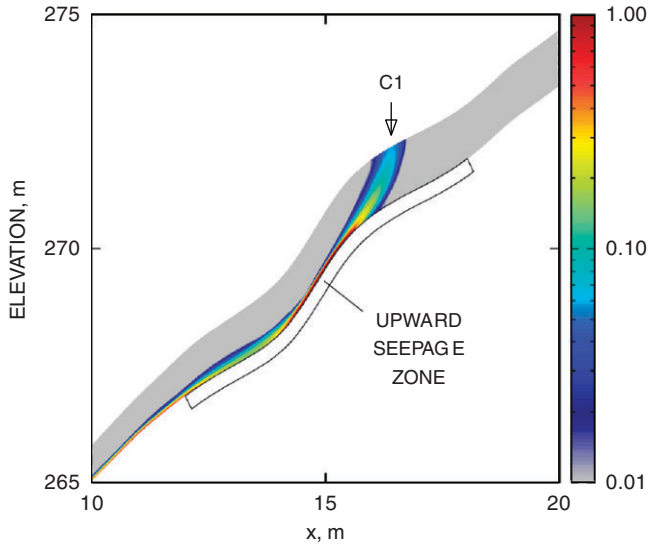

Figure 13. Extensional shear zone predicted by the hydro-mechanical model for an upward seepage of 100 mm/h for 2.5 h over the segment shown. A primary scarp zone developed at inflection point C1. Color bar is plastic strain in percent.

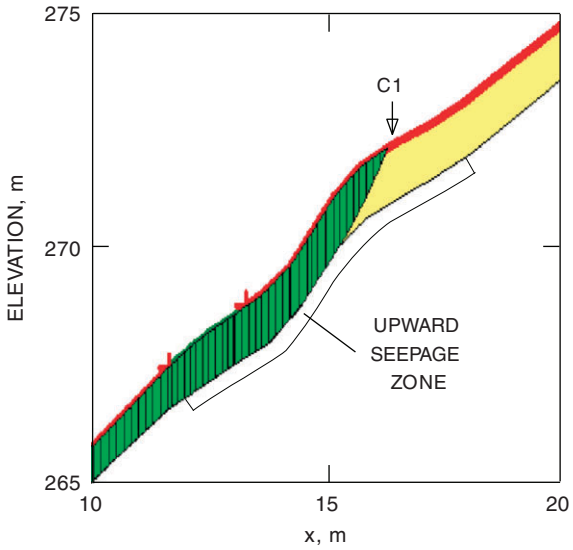

Figure 14. Extensional shear zone predicted by the limit-equilibrium model for an upward seepage of 100 mm/h for 2.5 h over the segment shown. A primary scarp zone developed at inflection point C1, in agreement with the continuum model. Factor of safety = 1.016 by Spencer's method.

6. CLOSURE

We have presented a methodology for quantifying deformation, stresses, saturation, fluid flow, and factor of safety for a steep hillside slope subjected to rainfall infiltration. The technique entails sequential calculations, first, with a physics-based hydro-mechanical continuum model to generate stresses, pore pressures, and deformation within a slope, and, second, with a limit-equilibrium solution that relies on the pore pressures calculated by the continuum model to determine the factor of safety and the critical failure surface. We find the pore pressure variation to be a strong

DOI: 10.1002/nag

link between the continuum and limit-equilibrium solutions: for the same pore pressure variation within the slope, the continuum and limit-equilibrium solutions consistently predicted the same scarp zone for a given slope. We have not presented sensitivity analyses on the effect of material parameters on the deformation and stability responses of the subject slope; in fact, such parametric studies were conducted in [3]. Material parameters such as the effective cohesion and friction angle of the sediment do impact the mechanical responses of a slope; however, they appear to influence the timing of failure for the most part, but not the failure mechanism itself. We find the slope topography and rainfall history to impact the slope failure mechanism to a great extent. The results of this work underscore the need for a physics-based simulation for an accurate prediction of the timing of failure as well as the associated failure mechanism for slopes subjected to rainfall infiltration.

ACKNOWLEDGEMENTS

This work is supported by the US National Science Foundation (NSF) under Contract Numbers CMMI-0824440 and CMMI-0936421 to Stanford University, and by Förderung der wissenschaftlichen Forschung (FWF) of Austria under Project Number L656-N22 to Universität für Bodenkultur.

REFERENCES

1. Iverson RM. Landslide triggering by rain infiltration. *Water Resources Research* 2000; **36**:1897–1910.
2. Lu N, Likos WJ. *Unsaturated Soil Mechanics*. Wiley: Hoboken, NJ, 2004.
3. Borja RI, White JA. Continuum deformation and stability analyses of a steep hillside slope under rainfall infiltration. *Acta Geotechnica* 2010; **5**:1–14.
4. Borja RI, White JA. Conservation laws for coupled hydro-mechanical processes in unsaturated porous media: theory and implementation. In *New Trends in the Mechanics of Geomaterials*, Laloui L (ed.), Chapter 8. ALERT O. Zienkiewicz Course. Iste Wiley: New York, 2010.
5. Ebel BA, Loague K, VanderKwaak JE, Dietrich WE, Montgomery DR, Torres R, Anderson SP. Near-surface hydrologic response for a steep, unchanneled catchment near Coos Bay, Oregon: 2. Physics-based simulations. *American Journal of Science* 2007; **307**:709–748.
6. Torres R. Unsaturated zone processes and the hydrologic response of a steep, unchanneled valley. *Ph.D. Dissertation*, University of California, Berkeley, 1997.
7. Borja RI. Cam-Clay plasticity, part V: a mathematical framework for three-phase deformation and strain localization analyses of partially saturated porous media. *Computer Methods in Applied Mechanics and Engineering* 2004; **193**:5301–5338.
8. Bishop AW. The principle of effective stress. *Teknisk Ukeblad* 1959; **106**:859–863.
9. Borja RI. On the mechanical energy and effective stress in saturated and unsaturated porous continua. *International Journal of Solids and Structures* 2006; **43**:1764–1786.
10. Borja RI, Koliji A. On the effective stress in unsaturated porous continua with double porosity. *Journal of the Mechanics and Physics of Solids* 2009; **57**:1182–1193.
11. Van Genuchten MT. A closed-form equation for predicting the hydraulic conductivity of unsaturated soils. *Soil Science Society of America Journal* 1980; **44**:892–898.
12. Ebel BA, Loague K, Borja RI. The impacts of hysteresis on variably-saturated hydrologic response and slope failure. *Environmental Earth Sciences* 2010; **61**:1215–1225.
13. White JA, Borja RI. Stabilized low-order finite elements for coupled solid-deformation/fluid-diffusion and their application to fault zone transients. *Computer Methods in Applied Mechanics and Engineering* 2008; **197**:4353–4366.
14. Spencer E. A method of analysis of embankments using parallel inter-slice forces. *Géotechnique* 1967; **17**:11–26.
15. Bishop AW. The use of the slip circle in the stability analysis of slopes. *Géotechnique* 1955; **5**:7–17.
16. Fan K, Fredlund DG, Wilson GW. An interslice force function for limit equilibrium slope stability analysis. *Canadian Geotechnical Journal* 1986; **23**:287–229.
17. Houlsby GT. The work input to an unsaturated granular material. *Géotechnique* 1997; **47**:193–196.
18. Borja RI, Lee SR. Cam-Clay plasticity, part I: implicit integration of elasto-plastic constitutive relations. *Computer Methods in Applied Mechanics and Engineering* 1990; **78**:49–72.
19. Nuth M, Laloui L. Effective stress concept in unsaturated soils: clarification and validation of a unified framework. *International Journal for Numerical and Analytical Methods in Geomechanics* 2008; **32**:771–801.
20. Varnes DJ. Slope movement types and processes. In *Landslides Analysis and Control*, Schuster RL, Krizek RJ (eds). Special Report 176. National Academy of Sciences: Washington, DC, 1978.

DOI: 10.1002/nag